energies

MDPI

Article

An Active Equalization Method for Lithium-ion Batteries Based on Flyback Transformer and Variable Step Size Generalized Predictive Control

Jianwen Cao, Bizhong Xia * and Jie Zhou

Tsinghua Shenzhen International Graduate School, Tsinghua University, Shenzhen 518055, China; jw-cao18@mails.tsinghua.edu.cn (J.C.); zhoujiesxh@foxmail.com (J.Z.)
* Correspondence: xiabz@sz.tsinghua.edu.cn; Tel.: +86-180-3815-3128

Abstract: The inconsistency in large-scale battery pack significantly degrades the performance of electric vehicles. In order to diminish the inconsistency, the study designs an active equalization method comprising of equalizer and equalization strategy for lithium-ion batteries. A bidirectional flyback transformer equalizer (BFTE) is designed and analyzed. The BFTE is controlled by a pulse width modulation (PWM) controller to output designated balancing currents. Under the purpose of shortening equalization time and reducing energy consumption during the equalization process, this paper proposes an equalization strategy based on variable step size generalized predictive control (VSSGPC). The VSSGPC is improved on the generalized predictive control (GPC) by introducing the Step Size Factor. The VSSGPC surmounts the local limitation of GPC by expanding the control and output horizons to the global equalization process without increasing computation owing to the Step Size Factor. The experiment results in static operating condition indicate that the equalization time and energy consumption are reduced by 8.3% and 16.5%, respectively. Further validation in CC-CV and EUDC operating conditions verifies the performance of the equalizer and rationality of the VSSGPC strategy.

Keywords: electric vehicle; battery equalization; flyback transformer; variable step size generalized predictive control; Step Size Factor

Citation: Cao, J.; Xia, B.; Zhou, J. An Active Equalization Method for Lithium-ion Batteries Based on Flyback Transformer and Variable Step Size Generalized Predictive Control. *Energies* **2021**, *14*, 207. https://doi.org/10.3390/en14010207

Received: 28 November 2020
Accepted: 29 December 2020
Published: 2 January 2021

1. Introduction

The rapid consumption of fossil fuel and accelerating global warming raises a worldwide concern of energy crisis and environmental problems. In this case, electric vehicles (EVs) are rapidly appreciated by governments, automobile manufacturers, consumers, and research institutions [1]. EVs can be divided into battery electric vehicles (BEVs), hybrid electric vehicles (HEVs), plug-in hybrid electric vehicles (PHEVs) and fuel cell electric vehicles (FCEVs) [2]. BEV accounts for the most substantial proportion of new energy vehicle production and sales. Besides, BEV owns a broad market potential because of its exceptional advantages of zero emission, low noise, and high efficiency. Compared with other types of batteries, the lithium-ion battery has the benefit of greater energy density, longer cycle life, and higher discharge rate [3]. Therefore, the lithium-ion battery is broadly used in EVs. Battery pack is the critical component of EVs and determines the driving range. To meet EV's huge energy demand, battery packs usually comprise of numerous cells. The pack must be appropriately managed to prolong cycle life, avoid safety accidents, and maximize available energy [4]. Therefore, a high-end battery management system (BMS) is critical to enhancing EV's performance. The functional module of BMS includes safety protection, battery state parameters estimation, and battery equalization.

The inconsistency of cells in a battery pack is inevitable due to manufacturing tolerance, ambient temperature variation and aging rate divergence. The cells vary in internal resistance, self-discharge rate, and capacity, leading to the state of charge (SoC) diversity

aggravating along with cyclic charging and discharging [5]. Cells' inconsistency degrades battery pack performance significantly thereby reducing the driving range of EVs. Figure 1 shows the charge and discharge process of the unbalanced battery string, which corresponds to EVs' charging and driving states. As the range of cells' SoCs enlarges, the total available capacity of the battery pack diminishes proportionally, leading to the degradation of EVs' driving range. Furthermore, the inconsistency of SoCs causes unbalanced charge and discharge depths. Those cells in a larger depth of charge (Cell 2, Figure 1) or discharge (Cell 3, Figure 1) are on the edge of overcharging and overdischarging for a longer period, which accelerates the cycle life decay rate of specific cells and ultimately leads to degradation of pack useful life. Accordingly, the service life of EVs decreases. Therefore, the Equalization technology should be applied in series-connected batteries to lessen unbalanced levels of batteries, expand the available capacity of battery packs, and improve the overall performance of EVs.

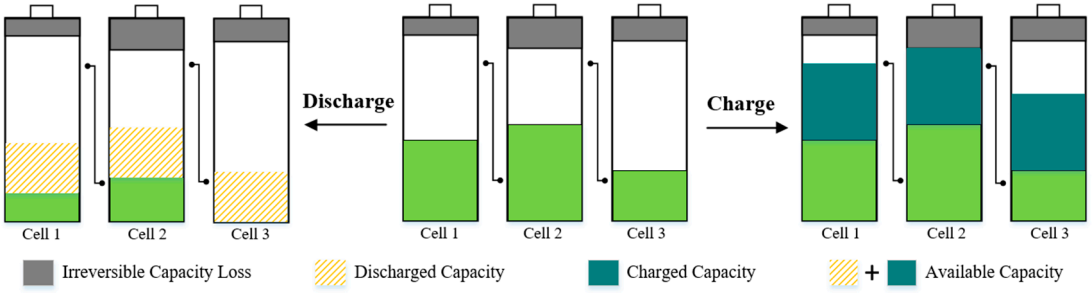

Figure 1. Charge and discharge of unbalanced battery string.

Battery equalizers are widely used in multi-battery systems to maintain balanced charge among cells [6]. Equalization topologies can be categorized into passive and active methods by the management of surplus energy [7]. The passive methods transform energy from cell to heat by shunting resistor. Fixed shunting resistor equalizer is the simplest method to implement due to its unnecessary control [8]. Switch shunting resistor equalizer connected or disconnect with cells by switches and therefore is more efficient than fixed shunting resistor equalizer [7]. Analog shunting resistor equalizer controls the resistors' connection status by voltage reference [9]. It has the advantage of unnecessary control but requires a relatively higher cost. The passive method is widely employed in the EV industry because of its low-cost, simple structure and convenient implementation. However, considerable heat emission caused by energy dissipation is the major setbacks of the passive method, which triggers a significant challenge of temperature management of the pack. Besides, the slow equalization speed makes the passive method unsuitable for the equalization of large-capacity power batteries.

Various non-dissipative active equalizers have been proposed to overcome the setbacks raised by passive methods. Categorized by energy transfer media, active equalizers can be classified in capacitor, inductor, and transformer based. Capacitor-based equalizers include switch capacitor equalizer, single-switch capacitor equalizer, and double-tiered switch capacitor equalizer. Switch capacitor equalizer has the advantages of a straightforward control strategy while it has multiple capacitors [10–12]. Single-switch capacitor equalizer has only one capacitor but requires complex control [13,14]. Double-tiered switch capacitor equalizer has an additional capacitor tiered for energy transfer, thereby increasing the equalization speed [15,16]. Capacitor-based equalizers have the advantages of good low-temperature characteristics, wide operating temperature range, high power density, and long cycle life. However, the practical application of capacitor-based equalizers is hindered by a relatively larger volume. Inductor-based equalizers operate on the principle of Buck-Boost. Single-inductor equalizers connect the highest and lowest cells with inductor alternately to transfer energy between cells but require complex and precise control [17]. Multi-inductor equalizers can only transfer energy from adjacent batteries and yet is no

need for complex control relatively [18]. In spite of the advantages of relatively higher balancing current and shorter operation time, inductor-based equalizers are challenging for the practical implementation of large-scale packs due to their high cost and inevitable magnetic losses [13]. Transformer-based equalizers include single-winding transformer equalizers, multi-winding transformer equalizers. Single-winding transformer equalizers contain only one transformer, which can reduce volume and cost, but has multiple switches, which lead to complex control [19,20]. Multi-winding transformer equalizers have fewer switches and require simpler control, but the large volume and, respectively, high cost should be concerned [13,21]. Besides, flyback structure [22] are generally selected for the primary and second winding of the transformer-based equalizers. The foremost challenge of transformer-based equalizers is winding matching which increases the complexity of equalizer design. Furthermore, the necessity of precise control in transformer-based equalizer enhances the difficulties of devising controllers. The high magnetic loss is also a limitation of transformer-based equalizer.

Flyback transformer is a special application of transformer. The flyback transformer is capable of providing high voltages using relatively few turns of windings. The main feature of flyback transformer is that its output gets energy when the primary winding is disconnected from the power supply. The flyback transformer is competent for DC-DC energy transfer due to its advantages of circuit simplicity, electric isolation, high efficiency and small turn ratio [23]. Under its advantages, flyback transformer has been utilized in numerous application areas, e.g., energy storage, energy supply and transfer, galvanic isolation [24] and photovoltaic application [25]. Thus, considering its strength in energy conversion, this paper devises the equalizer based on flyback transformer.

Equalization strategies play a significant role in pack balancing management since they determine the performance of the equalizer during the equalization process. Numerous strategies for equalization have been proposed based on the corresponding balancing topologies. For switch shunting resistor equalizer of passive methods, fuzzy logic control, which considers the thermal effect of the shunting resistors in the equalization process, can reduce equalization time and improve energy efficiency while maintaining low heat emission of the shunting resistors [26]. In the field of active methods, fixed duty cycle (FDC) methods [27,28] are used in transformer-based equalizers. FDC method is the most straightforward strategy but has no idea of regulating the balancing current. Those cells whose SoCs are higher or lower than the average value are discharged or charged at the maximum equalization current, respectively. The variable duty cycle (VDC) methods [29,30] have been employed to control the transformer-based equalizer. The main idea of VDC is regulating the balancing current and the applied duty cycles of VDC are proportional to SoC deviations from the average value. Besides, some intelligent control methods have been proposed to control the equalizers. Fuzzy logic control [31,32] has been applied for transformer- and inductor-based equalizers, achieving voltage balancing in a short period. Model predictive control [22,33] proves its competence in controlling transformer-based equalizers. This method improves the efficiency of equalization circuit and prolongs cell life. Game theory [34] has been successfully applied in inductor-based equalizer to realize SoC consistency in battery string, which reduces control complexity.

Equalization strategies can be further subdivided into voltage, SoC and remaining-capacity-based according to equalization reference. Voltage-based equalization strategies operate with the target of voltage uniformity. Fuzzy logic control strategy [31] applied in transformer-based equalizers considers voltage as reference. Battery cell voltage balancing control [35] employed in a modular bridge equalizer aims at voltage consistency. The control strategy of active hierarchical equalization circuits [36] achieves voltage consistency. Voltage-based equalization strategies are convenient to execute and greatly streamline the implementation of strategies because cells' voltages can be acquired straightforwardly. However, as the inconsistency of internal resistance in a battery string gradually grows due to aging rate divergence, the terminal voltage is no longer competent as equalization standard. During equalization procedures, those cells with larger internal resistance

appear to output higher terminal voltage under the same charging balancing current, or vice versa, making the terminal voltage an unreliable equalization criterion. Remaining-capacity-based strategies consider cell remaining capacity as balancing standard. An active equalization method based on the remaining capacity [37] is applied in transformers-based equalizers and an on-line equalization algorithm [38] which is embedded with the remaining-capacity estimation is used to balance the strings. The main challenge of remaining-capacity-based strategies is the unavailability of the cells' remaining capacities which are estimated by complicated online parameter identification algorithms. SoC-based equalization strategies take cells' SoCs as reference. Model predictive control, which is used in bidirectional transformer-based equalizer [22,33], takes SoC as reference. Fuzzy logic control [39] conducted in inductor-based equalizer aims to balance cell' SoCs. A data-stream-mining-based strategy [40] applied in single-switch capacitor equalizer attempts to equalize SoCs. By maintaining cells charging or discharging depth consistency, SoC-based equalization strategies can competently retard the aging of packs. Although SoC estimation precision influences the effect of equalization, SoC-based equalization strategies are preferable in virtue of its significant strength.

The research on the equalization method in this paper is aimed at the practical application in EVs. The working conditions of EVs can be generally divided into three states: parking, driving, and charging. First of all, the parking condition is the one with the longest time among the three states. The passive equalizer, which is vastly employed in practical application, provides small equalization currents thereby emerging a low speed [7]. Therefore, in practical applications, the passive equalizer runs during the parking condition. In this case, the proposed equalization method is researched and verified during the parking condition to study the energy transfer efficiency and speed of the equalizer under the control of the proposed equalization strategy. Secondly, EVs' performance of driving range is demonstrated in the driving condition. For the complex realistic driving environment [41], international standards stipulate a variety of experimental test methods to simulate realistic driving conditions, such as The Extra Urban Driving Cycle (EUDC), The Federal Urban Driving Schedule (FUDS) and The New European Driving Cycle (NEDC). When the battery pack is not uniform, the capacity cannot be completely released, leading to a decline in EVs' driving range. For the problem under the driving states, this research also applies the design and verification of the equalizer to the driving process to prolong the driving range of EVs. Finally, the commonly used charging method for EVs in charging conditions is the constant current constant voltage (CC-CV) method [42]. When the battery pack is under-charged and unbalanced, the battery cannot be fully charged because cells are limited by the charge cut-off voltage for safety. To study and address this problem, the proposed equalization method is also applied in the charging process to verify the effect of increasing the overall available capacity.

Under the conditions discussed above for the realistic application environment of EVs, the battery pack is separated from the electric vehicle as a studied object of the equalization method. The working conditions of the battery pack can be summarized as static, discharging, charging, which correspond to the parking, driving and charging states of EVs, respectively. Among them, the discharge condition is verified by EUDC, and the charging condition is tested in CC-CV. Besides, the large-scale battery pack in a realistic application of EVs enhances the design and research difficulty of equalizer [43]. To simplify the research complexity and simulate the actual use of large battery packs as much as possible, this study employed a series-connected battery string as the object of equalizer design and verification. In this environment, the key research and engineering aspects are to design the equalizer based on flyback transformer for battery string, study the energy transfer efficiency and speed under the control of equalization strategy in the static condition, and verify the applicability of the equalizer during the discharging and charging process to improve the maximum discharged capacity and available capacity.

The outline of this paper is as follows: Section 2 introduces the architecture and operating principles of BFTE. Section 3 presents the control of the equalizer. Section 4

designs the VSSGPC strategy improved from traditional GPC. Section 5 describes the experiment bench and discusses experiment results. Section 6 summarizes this article.

2. Bidirectional Flyback Transformer Equalizer

2.1. Equalizer Architecture

The architecture of bidirectional flyback transformer equalizer (BFTE), which is applicable for battery strings consisting i cells, is shown in Figure 2. The primary feature of BFTE is the ability to transfer energy between cells and battery string bidirectionally. BFTE can be structured in several sub-modules, and each sub-module connects specific cell with battery string separately. The blue part of Figure 2 highlights the first equalizer sub-module, mainly composed of a flyback transformer (*T1*), two MOSFETs (*MOS1*, *MOS1′*), two current feedback resistors (*R1*, *R1′*). Each equalizer sub-module needs two pulse width modulation (PWM) signals to control MOSFETs. Therefore, the recommended controller should be equipped with at least 2i PWM channels to meet the need of BFTE.

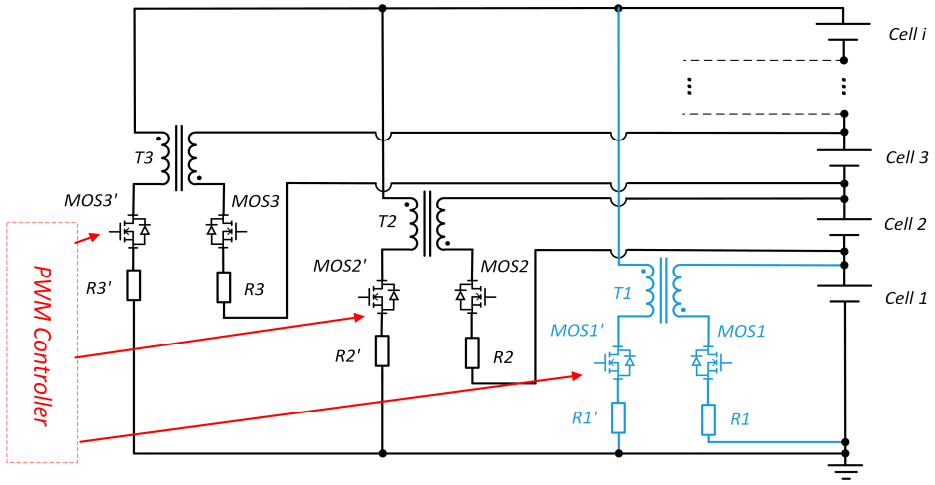

Figure 2. The architecture of a bidirectional flyback transformer equalizer (BFTE).

2.2. Operating Principle

This section discusses the operating principle of BFTE. As shown in Figure 3, *Cell i* is separated from the battery string to clarify the explanation. *MOS i* and *MOS i′* are controlled by PWM channel *GiP* and *GiS*. *IiP* and *IiS* are the current sensing channels. The operating modes can be divided into Cell-to-String (C2S) Mode and String-to-Cell (S2C) Mode.

2.2.1. C2S Mode

In C2S Mode, *Cell i* is discharged and then battery string is charged. Firstly, *MOS i* is turned on. Figure 3a describes the process of *Cell i* being discharged, which can be expressed as:

$$L_i(i_p - i_0) = U_i \cdot t_{on} \tag{1}$$

where U_i is voltage of *Cell i*, L_i represents inductance of primary winding, t_{on} represents conduction time of *MOS i*, i_0 and i_p represent initial primary current and primary current, respectively.

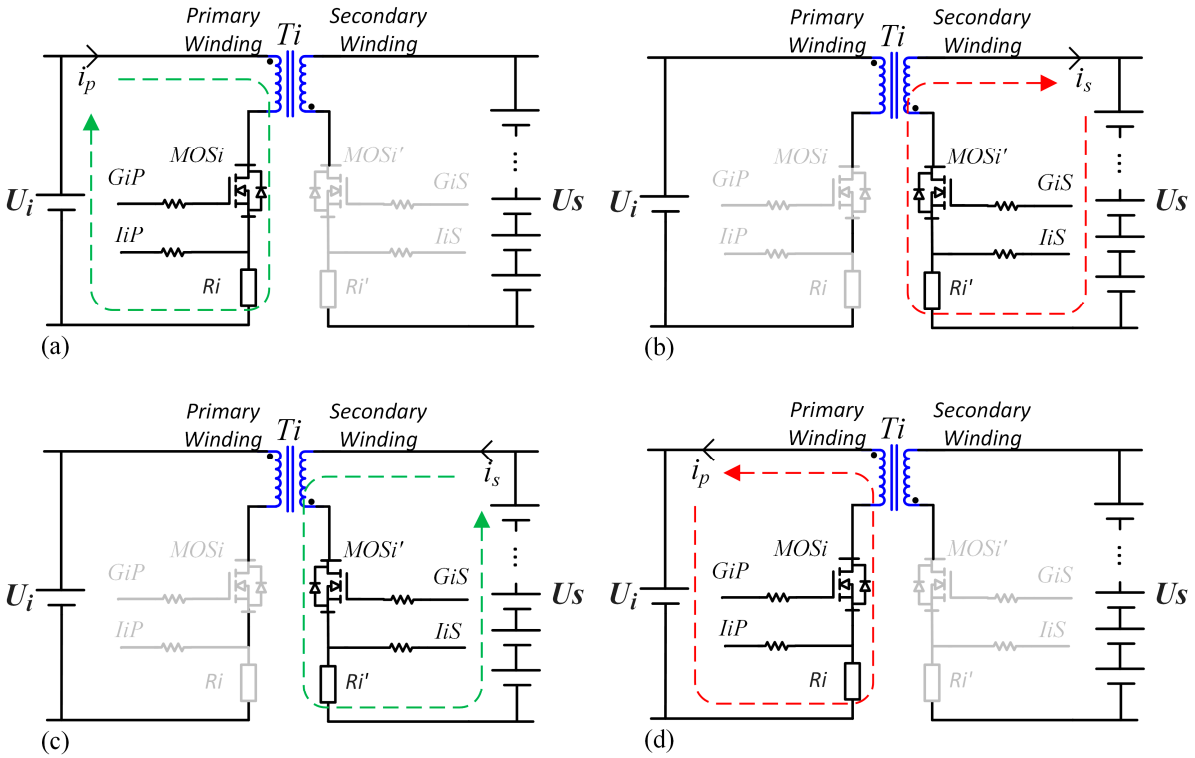

Figure 3. Equalizer operating modes; (**a**) cell-to-String (C2S) mode: cell is discharged; (**b**) C2S mode: string is charged; (**c**) S2C mode: string is discharged; (**d**) S2C mode: cell is charged.

MOS i is turned off when i_p reach peak current I_p, which is set by feedback current resistor (*Ri*, Figure 3a) and sensed by channel *IiP*. Generally, the initial primary current i_0 is equal to zero.

$$i_p = I_p,\ i_0 = 0 \tag{2}$$

As shown in Figure 3b, once the *MOS i* is turned off and *MOS i'* is turned on, the primary winding is opened. Current following in primary winding decreases to zero rapidly, leading to the sudden change of magnetic flux in transformer *Ti*. As a consequence, reversed current i_i' is induced in the secondary winding. The secondary charging process can be described by:

$$\begin{cases} L_i'(-i_s + i_i') = S \cdot U_i \cdot t_{on}' \\ S = \frac{U_s}{U_i},\ i_i' = \frac{I_p}{T} \end{cases} \tag{3}$$

where L_i' is inductance of secondary winding, i_s is secondary current, U_s represents string voltage, t_{0n}' is conduction time of *MOS i'*, T is turn ratio of secondary and primary windings.

When i_s meet the following condition, *MOS i'* is shut down.

$$i_s = 0 \tag{4}$$

In single operating circle, the discharging current $I_{p\_discharge}$ of *Cell i* and charging current I_{s_charge} of battery string can be derived from Equations (1)–(4) and expressed as:

$$\begin{cases} I_{p\_discharge} = \frac{\overline{i_p} \cdot t_{on} - \overline{i_s} \cdot t_{on}'}{t_{on} + t_{on}'} = \frac{1}{2} I_p \frac{S-1}{S+T} \\ I_{s\_charge} = \frac{\overline{i_s} \cdot t_{on}'}{t_{on} + t_{on}'} = \frac{1}{2} I_p \frac{1}{S+T} \eta_1 \end{cases} \tag{5}$$

where η_1 is the energy transfer efficiency of C2S Mode.

Equation (5) describes the theoretical calculation of average current in a single operating circle which is microsecond level. As mentioned above, the equalizer is controlled by a set of PWM signals provided by a specific controller. Therefore, the average current during a relatively longer period of time is proportional to the duty ratio of PWM signals and can be described as:

$$\begin{cases} I_{p\_dis} = I_{p\_discharge} \cdot D_i \\ I_{s\_cha} = I_{s\_charge} \cdot D_i \end{cases} \tag{6}$$

where I_{p_dis} and I_{s_cha} represent average current in primary and secondary windings of macroscale time, D_i is duty ratio.

2.2.2. S2C Mode

In S2C Mode, string is discharged and then *Cell i* is charged. As shown in Figure 3c,d, the acting sequence of *MOS i* and *MOS i'* is reversed compared with C2S Mode. The analysis of S2C Mode is similar to the derivation of C2S Mode above. Therefore, the analysis results are given directly as following equations:

$$\begin{cases} I_{p\_charge} = \frac{1}{2} I_p \frac{(S-1)T}{S+T} \eta_2 \\ I_{s\_discharge} = \frac{1}{2} I_p \frac{T}{S+T} \end{cases} \tag{7}$$

where I_{p_charge} and $I_{s\_discharge}$ represent charging current of primary winding and discharging current of secondary winding in single operating circle, and η_2 is the energy transfer efficiency of S2C Mode.

In control of PWM signals, the average current in primary and secondary windings of macroscale time I_{p_cha}, I_{s_dis} are described as:

$$\begin{cases} I_{p\_cha} = I_{p\_charge} \cdot D_i \\ I_{s\_dis} = I_{s\_discharge} \cdot D_i \end{cases} \tag{8}$$

3. Control of Equalizer

3.1. Equalization System and Control Target

BFTE and battery string constitute the equalization system and are the controlled object. Because BFTE is controlled by the PWMs to equalize the string, the PWM signals are considered as the control signals of the equalization system. The SoCs of cells are observed and considered as the equalization reference. Hence, the SoC is selected as the outputs. The controlling effect is evaluated by equalization time and energy loss, which are described by the terminal and processual target.

3.1.1. Inputs

Inputs of the equalization system are the normalized equalization currents controlled by PWM signals. According to the architecture of BFTE, the number of inputs is equal to the number of cells. The *i*-th input u_i is expressed as:

$$u_i = \frac{I_i}{I_{i\max}}, \ |u_i| = D_i, \ u_i \in [-1, 1] \tag{9}$$

where $I_{i\max}$ is the maximum equalization current limited by BFTE, I_i represents equalization current regulated by the equalization strategy, and D_i is the duty ratio in Equations (6) and (8).

3.1.2. Outputs

The outputs of the equalization system should reveal the inconsistency level of the battery string. SoC is a competent standard for the unbalanced level and should be considered as the output. Accordingly, the number of outputs is equal to the number

of cells. The estimation of SoCs will not be discussed in this paper. The i-th output is expressed as:

$$y_i = SoC_i,\ y_i \in [0,1] \tag{10}$$

3.1.3. Terminal Control Target

In this study, when the variance of SoCs is less than 1×10^{-6}, the cells are considered to be consistent. Therefore, as the following terminal control target is satisfied, the equalization process will be terminated.

$$D\{y(T_c)\} < 1 \times 10^{-6} \tag{11}$$

where T_c is the equalization time when all cells are considered to be consistent, and indicates the equalization speed.

3.1.4. Processual Control Target

An excellent equalization strategy should be characterized by low energy loss and short equalization time. The Processual control target is minimizing both equalization time and energy loss during SoCs converging. Hence, a cost function $J(u)$, the weighted sum of equalization time and energy loss, is employed to evaluate the control effect. Processual control target is described as:

$$\min J(u) \tag{12}$$

where

$$J(u) = T_c + \lambda E \tag{13}$$

E represents processual energy loss which can be calculated by Equation (46). λ is the weighting factor.

3.2. The Challenges of Equalization Strategy

Under the purpose of achieving higher energy transition efficiency and faster equalization speed, equalization strategy applied in BFTE is challenging. The challenges of equalization strategy mainly embody the following three aspects.

3.2.1. Multiple Inputs

For a battery string consisting of i cells, BFTE is controlled by 2i PWM signals. Note that a pair of PWMs for one cell is complementary. Therefore, the equalization system of i cells requires i independent inputs, the multiplicity of which significantly complicates the balancing controlling procedures.

3.2.2. Coupling System

The discussion in Section 2 indicates that, while one cell being discharged or charged, the other cells, rather than stay still, are charged or discharged. This phenomenon reveals that the equalization system is coupling, making it tricky to control the cells' SoCs separately.

3.2.3. Inputs Constraints

The inputs of the equalization system are restricted by channel currents amplitudes and interactions, which are determined by the hardware of BFTE. For the safety of the equalizer, the maximum number of simultaneously open channels should be limited. The constraints, which are described in Section 4.2 in detail, hamper the solutions to the optimum control law.

4. Variable Step Size Generalize Predictive Control

This section introduces the proposed variable step size generalized predictive control (VSSGPC) strategy in the following order. Firstly, Section 4.1 discusses the basic derivation of generalized predictive control (GPC) for the equalization system. Secondly, Section 4.2

solves the optimum control law of GPC with constrained inputs. Thirdly, Section 4.3 settles the problem of undetermined system parameters in CARIMA model. Finally, Section 4.4 introduces the principles of the improved VSSGPC and the physical significant of the introduced Step Size Factor.

4.1. Generalized Predictive Control

4.1.1. The Basic Concept of GPC

The schematic of GPC is illustrated in Figure 4. Limited control and output horizons are adopted to stand for the global control process. At time k, the cost function $J(k)$ is calculated based on predicted outputs Y. With a target of minimizing $J(k)$, projected controls U are obtained by optimization algorithms discussed in Section 4.2. The first row of projected controls matrix U at present time k is accepted as the optimum control law for the current moment. As the process rolls to the next moment $k+1$, the optimum control law is acquired by the same method.

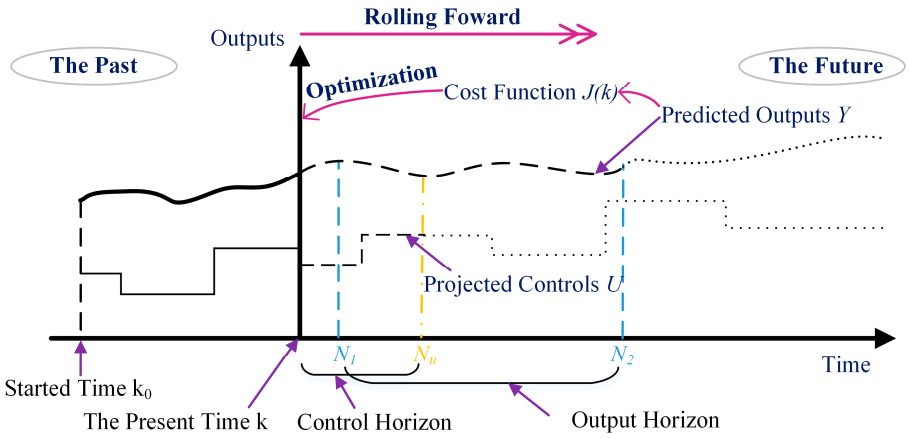

Figure 4. Schematic of generalized predictive control (GPC).

4.1.2. GPC of SISO System

For clarity, GPC of single-input-single-output (SISO) system is discussed first. SISO CARIMA model can be described by the following difference equation:

$$A(z^{-1})y(k) = B(z^{-1})u(k-1) + \frac{C(z^{-1})\xi(k)}{\Delta} \tag{14}$$

where

$$\begin{cases} A(z^{-1}) = 1 + a_1 z^{-1} + \cdots + a_{n_a} z^{-n_a} \\ B(z^{-1}) = b_0 + b_1 z^{-1} + \cdots + b_{n_b} z^{-n_b} \\ C(z^{-1}) = c_0 + c_1 z^{-1} + \cdots + c_{n_c} z^{-n_c} \end{cases} \tag{15}$$

$y(k)$ and $u(k-1)$ represent output and input of the controlled object, respectively. $\xi(k)$ is white noise sequence with zero mean. z^{-1} is backward shift operator, that is $z^{-1}y(k) = y(k-1)$. Δ is difference operator, defined as $\Delta = 1 - z^{-1}$. k represents the present moment. n_a, n_b and n_c represent the orders of Equation (15)

The following Diophantine Equation (16) is considered.

$$1 = E_j(z^{-1})A(z^{-1})\Delta + z^{-j}F_j(z^{-1}) \tag{16}$$

The SISO prediction model, derived from Equations (14) and (16), is expressed as Equation (17). Reference [44] has given out detailed derivation of SISO prediction model, and the recursion of the Diophantine Equation. In order to avoid repetition, the derivation

of the SISO prediction model and the recursion of the matrices G, H and F is not discussed in this article.

$$\overrightarrow{y}(k|k) = G\Delta\overrightarrow{u}(k|k) + H\Delta\overleftarrow{u}(k) + F\overleftarrow{y}(k) \tag{17}$$

where

$$\begin{cases} \overrightarrow{y}(k|k) = [y(k+N_1|k), y(k+N_1+1|k), \cdots, y(k+N_2|k)]^T \\ \Delta\overrightarrow{u}(k|k) = [\Delta u(k|k), \Delta u(k+1|k), \cdots, \Delta u(k+N_u-1|k)]^T \\ \Delta\overleftarrow{u}(k) = [\Delta u(k-1), \Delta u(k-2), \cdots, \Delta u(k-n_b)]^T \\ \overleftarrow{y}(k) = [y(k), y(k-1), \cdots, y(k-n_a)]^T \end{cases} \tag{18}$$

N_1 and N_2 represent the minimum and maximum output horizons. N_u is the control horizon. At the present moment k, $\overrightarrow{y}(k|k)$ and $\overrightarrow{u}(k|k)$ are the output and input in the future. Specifically, $y(j|k)$ is considered as the predicted output y at future time j calculated by the present and previous input and output. $\overleftarrow{y}(k)$ and $\overleftarrow{u}(k)$ are the output and input in the past, which were recorded.

4.1.3. GPC of MIMO System

As described in Section 3, BFTE should be considered as a multi-input-multi-output (MIMO) system. Therefore, the MIMO CARIMA model is built and described as:

$$\widetilde{A}(z^{-1})Y(k) = \widetilde{B}(z^{-1})U(k-1) + \frac{\widetilde{C}(z^{-1})\xi(k)}{\Delta} \tag{19}$$

where

$$\begin{cases} \widetilde{A}(z^{-1}) = diag\{A_1(z^{-1}), \cdots, A_r(z^{-1})\} \\ \widetilde{B}(z^{-1}) = \begin{bmatrix} B_{11}(z^{-1}) & B_{12}(z^{-1}) & \cdots & B_{1m}(z^{-1}) \\ B_{21}(z^{-1}) & B_{22}(z^{-1}) & \cdots & B_{2m}(z^{-1}) \\ \vdots & \vdots & \ddots & \vdots \\ B_{r1}(z^{-1}) & B_{r2}(z^{-1}) & \cdots & B_{rm}(z^{-1}) \end{bmatrix} \\ A_i(z^{-1}) = 1 + a_i z^{-1},\ i = 1, \cdots, r \\ B_{ij}(z^{-1}) = b_{ij,0} + b_{ij,1}z^{-1} + b_{ij,2}z^{-2},\ i = 1, \cdots, r,\ j = 1, \cdots, m \end{cases} \tag{20}$$

m and r represent the numbers of inputs and outputs of the equalization system. a_i, $b_{ij,0}$, $b_{ij,1}$ and $b_{ij,2}$ are the system parameters recognized by recursive least-squares discussed in Section 4.3.

The GPC prediction model of MIMO system is an extension of SISO model. Based on the idea of the superposition principle, the derivation of MIMO prediction model is discussed in three steps.

Step 1: Under the assumption that only the input j changes and other inputs remain zero, the prediction model of output i is considered as:

$$\overrightarrow{y}_{ij}(k|k) = G_{ij}\Delta\overrightarrow{u}_j(k|k) + H_{ij}\Delta\overleftarrow{u}_j(k) + \sum_{l=1}^{r} F_{il}\overleftarrow{y}_l(k) \tag{21}$$

Output i represents the SoC of *Cell i*. Noted that the predicted output $\overrightarrow{y}_{ij}(k|k)$ is independent from other outputs $\overleftarrow{y}_l(k)$ $(i \neq l)$ in the past. Therefore, the matrix F is considered as:

$$F_{il} = 0, i \neq l \tag{22}$$

Considering Equation (22), the prediction model (21) can be simplified as:

$$\overrightarrow{y}_{ij}(k|k) = G_{ij}\Delta\overrightarrow{u}_j(k|k) + H_{ij}\Delta\overleftarrow{u}_j(k) + F_{ii}\overleftarrow{y}_i(k) \tag{23}$$

Equation (23) describes the prediction model of input j and output i. By analogy with prediction model (17), the relationship can be considered as a SISO system as shown in Equation (24). For each pair of input and output combination, the form of SISO prediction

model is adopted. Therefore, as discussed in Section 4.1.2, the matrixes G_{ij}, H_{ij}, F_{ii} can be solved.

$$A_i(z^{-1})y_{ij}(k) = B_{ij}(z^{-1})u_j(k-1) + \frac{C_{ij}(z^{-1})\xi(k)}{\Delta} \tag{24}$$

Step 2: Under the assumption that all inputs change, and the superposition principle is considered. Output i can be described as:

$$\overrightarrow{y}_i(k|k) = \sum_{j=1}^{m} G_{ij}\Delta\overrightarrow{u}_j(k|k) + \sum_{j=1}^{m} H_{ij}\Delta\overleftarrow{u}_j(k) + F_{ii}\overleftarrow{y}_i(k) \tag{25}$$

where

$$\overrightarrow{y}_i(k|k) = [y_i(k+N_1|k), y_i(k+N_1+1|k), \cdots, y_i(k+N_2|k)]^T \tag{26}$$

Step 3: All inputs and outputs are considered. The prediction model can be expressed as:

$$Y(k|k) = \widetilde{G}\Delta U(k|k) + \widetilde{H}\Delta\overleftarrow{U}(k) + \widetilde{F}\overleftarrow{Y}(k) \tag{27}$$

where

$$\begin{cases} \widetilde{G} = \begin{bmatrix} G_{11} & G_{12} & \cdots & G_{1m} \\ G_{21} & G_{22} & \cdots & G_{2m} \\ \vdots & \vdots & \ddots & \vdots \\ G_{r1} & G_{r2} & \cdots & G_{rm} \end{bmatrix}, \widetilde{H} = \begin{bmatrix} H_{11} & H_{12} & \cdots & H_{1m} \\ H_{21} & H_{22} & \cdots & H_{2m} \\ \vdots & \vdots & \ddots & \vdots \\ H_{r1} & H_{r2} & \cdots & H_{rm} \end{bmatrix} \\ \widetilde{F} = diag(F_{11}, F_{22}, \cdots, F_{rr}) \end{cases} \tag{28}$$

$$\begin{cases} Y(k|k) = [y(k+N_1|k), y(k+N_1+1|k), \cdots, y(k+N_2|k)]^T \\ \Delta U(k|k) = [\Delta u(k|k), \Delta u(k+1|k) \cdots, \Delta u(k+N_u-1|k)]^T \\ \overleftarrow{Y}(k) = [y(k), y(k-1), \cdots, y(k-n_a)]^T \\ \Delta\overleftarrow{U}(k) = [\Delta u(k-1), \Delta u(k-2), \cdots, \Delta u(k-n_b)]^T \\ y = [y_1, y_2, \cdots, y_r]^T \\ u = [u_1, u_2, \cdots, u_m]^T \end{cases} \tag{29}$$

$Y(k|k)$ is the predicted output. $U(k|k)$ is the future input. $\overleftarrow{Y}(k)$ and $\overleftarrow{U}(k)$ are the past output and input, respectively. The elements G_{ij}, H_{ij} and F_{ii} in matrixes $\widetilde{G}$, $\widetilde{H}$ and $\widetilde{F}$ can be calculated separately from Equation (24) as a SISO model. Therefore, the prediction model is settled.

The prediction model (27) is used to generate a set of predicted output $Y(k|k)$ depend in part on future input $U(k|k)$ which are to be determined.

4.1.4. Cost Function

The cost function, which is the optimization target of the balancing process, is calculated by the predicted output $Y(k|k)$ and future input $U(k|k)$ of Equation (27), and is defined as:

$$J(k) = \sum_{j=0}^{N_2-N_1} W(j)^T W(j) + \sum_{j=1}^{N_u} \lambda(j)E(j)^T E(j) \tag{30}$$

where

$$\begin{cases} W(j) = y(k+j|k) - Y_s(k+j) \\ E(j) = U_v\eta u(k+j-1|k) \end{cases} \tag{31}$$

In the consideration of the ultimate goal of SoC unification, the reference output $Y_s(k+j)$ is set to the average of current SoCs. η and U_v represent energy transfer loss ratio matrix and cell terminal voltage matrix, respectively. $\lambda(j)$ is the weighting sequence.

The physical significance of $J(k)$ is maximizing the equalization speed at a lower cost of energy loss. Explicitly, the former and latter items of the cost function (30), which is

weighted by $\lambda(j)$, indicate the variance of SoCs from time $k+N_1$ to time $k+N_2$, and the energy loss of equalization process from time k to time $k+N_u$, respectively.

Table 1 summarizes the major parameters adopted in GPC.

Table 1. Parameters of generalized predictive control (GPC).

Parameter	Implication	Value	Parameter	Implication	Value
r	Number of outputs	6	m	Number of inputs	6
N_1	Output horizon	1	N_u	Control horizon	5
N_2		10	$\lambda(j)$, j = 1,...,6	Weighting sequence	0.1

4.2. Constraints Management and Optimum Control Law Solution

The solution to the optimum control law under constraints is introduced. The optimum control law at the present time k cannot be deduced directly because of the constrained inputs. Specifically, inputs of the equalization system are restricted by amplitude and interactions.

$$\begin{cases} \min J(k) \\ s.t. -1 \le u_i \le 1,\ i = 1, \cdots, m & C(1) \\ \sum\limits_{i=1}^{m} |sign(u_i)| \le MO & C(2) \end{cases} \tag{32}$$

The optimization problem can be expressed as:

$J(k)$: The cost function described by Equation (30).
$C(1)$: The amplitude restriction of inputs.
$C(2)$: The mutual influence between the inputs. The maximum number (MO) of equalizer sub-modules operating synchronously is limited for safety. MO is set to 4.

The optimization problem described by Equation (32) is a quadratic programming problem. There are plenty of methods to solve the quadratic problem with constraints, such as penalty function method, feasible direction method and active set method. However, they are competent to cope with $C(1)$, but not $C(2)$. This study employs the multi-population genetic algorithm (MPGA) to cope with optimization problems with both $C(1)$ and $C(2)$. The competences of MPGA lie in two aspects. Firstly, the encoding of inputs solves $C(1)$ automatically. Secondly, $C(2)$ can be dealt with by introducing the Fatal Factor in the fitness function.

Fatal Factor is defined as:

$$FF = ff^{NG} \tag{33}$$

where

$$ff = \begin{cases} 1.01, \sum\limits_{i=1}^{m} |sign(u_i)| > MO \\ 1, \sum\limits_{i=1}^{m} |sign(u_i)| \le MO \end{cases} \tag{34}$$

NG is the generations of genetic algorithm.

The fitness function of MPGA is defined as:

$$F(k) = FF \cdot J(k) \tag{35}$$

Under the influence of the Fatal Factor FF, which is exponential function of the generations NG, the fitness function $F(k)$ creates lower selective pressure in the initial stage of evolution. However, $F(k)$ creates increasing pressure as the population evolves, eliminating those individuals out of constraints in the late stage of evolution. As a consequence, the optimization problem with $C(2)$ is settled.

The basic steps of genetic algorithm can be sorted as encoding, crossover, mutation, selection, which will not be described in detail in this paper. Tables 2 and 3 display the choices of methods and parameters.

Table 2. Methods choices of genetic algorithm.

Steps	Encoding	Crossover	Selection
Method	Binary encoding	Multi-point crossover	Linear ranking selection

Table 3. Parameters choices of genetic algorithm.

Parameters	Values	Parameters	Values
Population Size	50	Mutation Probability	0.01
Bit String Size	$5mN_u$ [1]	Maximum Generations	350
Crossover Probability	0.95	Populations	10

[1] m is the number of input and N_u is the control horizon. The values of m and N_u are displayed in Table 1.

4.3. Adaptive Control and Parameter Estimation

Since the parameters of CARIMA model (19) in previous discussion remain undetermined, this section introduces the estimation method of the system parameters. GPC has the characteristics of adaptive control. The idea of adaptive control in this study lies in two aspects. Firstly, the initial parameters of CARIMA model need to be estimated for the construction of the prediction model (27). Secondly, the parameters should be adjusted due to the inevitable model errors and environmental interference during the control process. This paper adopts recursive least-squares to estimate the parameters of CARIMA model.

The data vector $\varphi_i^T(k)$ and parameter vector θ_i^T are defined as:

$$\begin{cases} \varphi_i^T(k) = [-y_i(k-1), u^T(k-1), \cdots, u^T(k-3)] \\ \theta_i^T = [a_{i,1}, b_{i1,0}, \cdots, b_{im,0}, \cdots, b_{i1,2}, \cdots, b_{im,2}] \end{cases} \tag{36}$$

The Equation (19) can be rewritten as:

$$y_i(k) = \theta_i^T \varphi_i(k) + \xi(k), i = 1, \cdots, m \tag{37}$$

Recursive least-squares (RLS) are used to estimate the parameter vector θ_i^T.

$$\begin{cases} \hat{\theta}_i(k) = \hat{\theta}_i(k-1) + \mu_i(k)[y_i(k) - \hat{\theta}_i^T(k-1)\varphi_i(k)] \\ \mu_i(k) = P_i(k-1)\varphi_i^T(k)[1 + \varphi_i^T(k)P_i(k-1)\varphi_i(k)]^{-1} \\ P_i(k) = P_i(k-1) - \mu_i(k)\varphi_i^T(k)P_i(k-1) \end{cases} \tag{38}$$

where $\hat{\theta}_i(k)$ is the estimation of data vector θ_i^T.

The iteration initial values are set as:

$$\hat{\theta}_i(0) = \mathbf{0}, P_i(0) = 10^7 I \tag{39}$$

4.4. Variable Step Size

This section proposes the variable step size generalized predictive control (VSSGPC) to improve the control effect of GPC.

The limitation of GPC is that it optimizes the overall control process by applying the optimum input of limited horizons, leading to a non-global optimization of the control process. The parameters N_1, N_2 and N_u can be increased to expand the control and output horizons and consequently better control effect of the whole equalization process can be obtained. However, due to the curse of dimensionality, the enlargement of horizons will

result in an exponential growth of computation, increasing the real-time implementation difficulty.

To solve the intractable dilemma of GPC, VSSGPC is proposed to enlarge the control and output horizons while maintaining a relatively low computation. The Step Size Factor ST is introduced in GPC to adjust the steps of horizons. The schematic of VSSGPC is illustrated in Figure 5. At the early stage of the control process (time k1), the step is enlarged by ST. Consequently, the control and output horizons are stretched. As time moves forward (time k2, k3), the control and output horizons are adjusted.

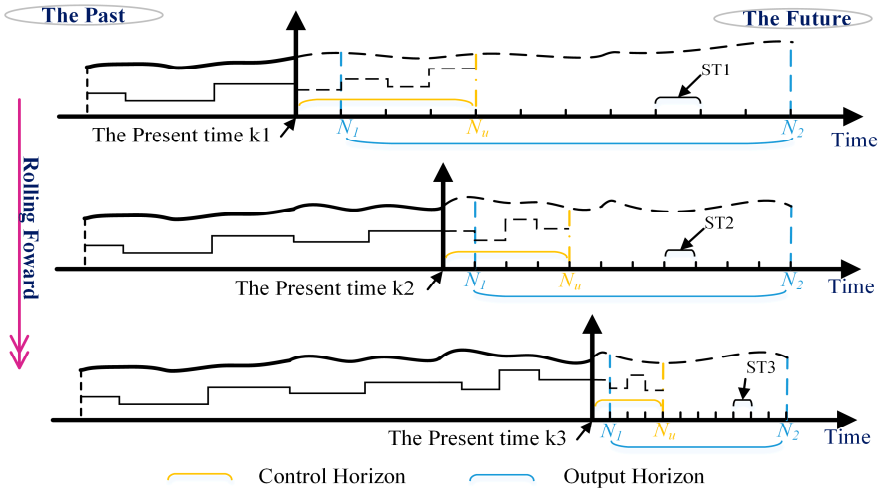

Figure 5. The schematic of variable step size generalized predictive control (VSSGPC).

ST is defined as:

$$ST = \Pi(\frac{T_t}{N_2 - N_1 + 1}) \tag{40}$$

where

$$T_t = \frac{\max\{y - E(y)\}Q}{I_{\max}} \tag{41}$$

The physical significance and rationality of ST is discussed. T_t represents the expected terminal time. According to the definition of SoC (the output y), T_t can be calculated by the maximum deviation of outputs, typical capacity of cells Q, and maximum channel balancing current $I_{\max}$, as described by Equation (41). ST represents the average step size of reaching T_t in $N_2 - N_1 + 1$ steps. ST is introduced to the prediction model (27) and the Equation (29) is rewritten as:

$$\begin{cases} Y(k|k) = [y(k+N_1|k), y(k+N_1+ST|k), \cdots, y(k+N_1+ST(N_2-N_1)|k)]^T \\ \Delta U(k|k) = [\Delta u(k|k), \Delta u(k+ST|k), \cdots, \Delta u(k+ST(N_u-1)|k]^T \\ \overleftarrow{Y}(k) = [y(k), y(k-ST), \cdots, y(k-ST{\cdot}n_a)]^T \\ \overleftarrow{\Delta U}(k) = [\Delta u(k-ST), \Delta u(k-2ST), \cdots, \Delta u(k-ST{\cdot}n_b)]^T \end{cases} \tag{42}$$

where

$$\begin{cases} \Delta u(k) = \Delta u(1), & k \le 0 \\ y(k) = y(1), & k \le 0 \end{cases} \tag{43}$$

Equation (42) indicates that the time domains of the past and future are extended backward and forwards, respectively. The predicted output $Y(k|k)$ can be stretched to the expected terminal time T_t, resulting in the global optimization of the control process.

The cost function (30) is revised as:

$$J(k) = \sum_{j=0}^{N_2-N_1} W\prime(j)^T W\prime(j) + \sum_{j=1}^{N_u} \lambda(j) E\prime(j)^T E\prime(j) \tag{44}$$

where

$$\begin{cases} W'(j) = y(k+N_1+ST{\cdot}j|k) - Y_s(k+N_1+ST{\cdot}j) \\ E'(j) = U_v \eta u(k+(j-1)ST|k) \end{cases} \tag{45}$$

The flow chart of VSSGPC is shown in Figure 6.

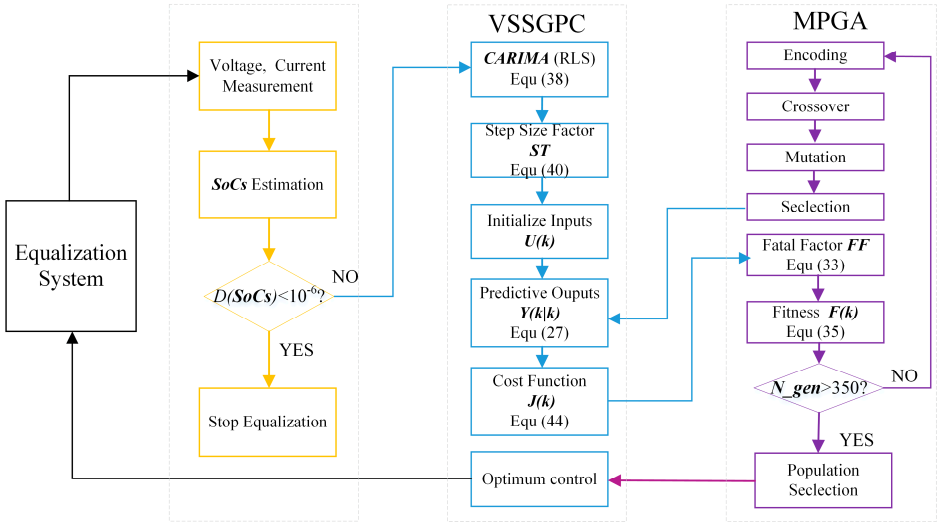

Figure 6. Flow chart of VSSGPC.

5. Experiment and Discussion

5.1. Experiment Bench

To testify the effectiveness of BFTE and VSSGPC strategy, this section designs and builds an experiment bench. The experimental battery string consists of 6 Lithium Cobalt Oxide batteries (ICR18650-33G SAMSUNG SDI). Details about the batteries are listed in Table 4. The equalizer controller is LTC3300-1, a controlling chip developed by Linear Technology Corporation. The string is charged and discharged by DC Power Supply Source (Chroma 6200L) and DC Electronic Load (Chroma 63200E). Voltages and currents are collected by the data acquisition board, whose measurement accuracy is $\pm 0.2\%$ and sampling time is 1 s. The current and voltage data are transmitted to PC. The optimum control law is resolved in MATLAB 2018b. After the resolution is finished, the control signals are transmitted to the equalizer. The calculation time for each step of GPC and VSSGPC is 1.78 s on average. The control signals are renewed every 4 s. Figure 7 shows the schematic diagram of the test bench.

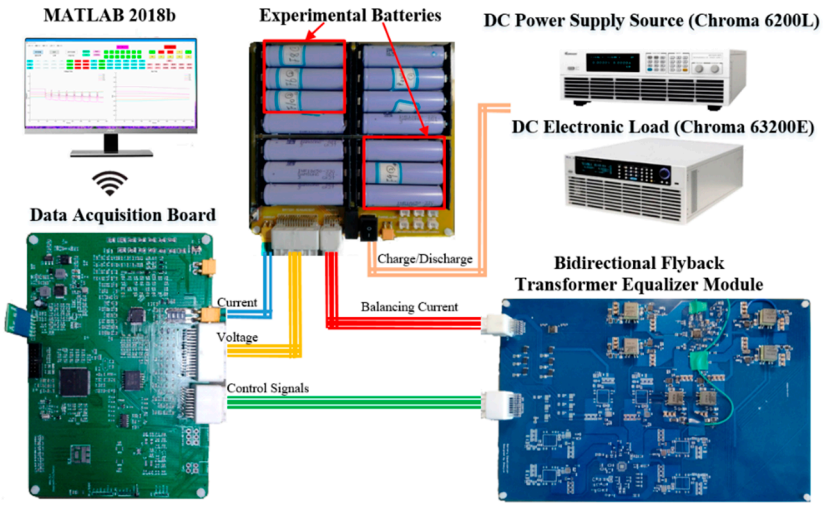

Figure 7. Schematic of experimental bench.

Table 4. Specifications of the tested battery.

Item	Specification	Item	Specification
Battery Model	ICR 18650-33G	Max. Charging Current	3 A (5 s)
Typical Capacity	2700 mAh	Max. Discharge Current	15 A (5 s)
Nominal Voltage	3.6 V	Discharge Cut-off voltage	2.5 V
Charging Voltage	4.1 V	Time between C/D	2 h
Charging Method	CC-CV	Test Temperature	25 °C

5.2. Static Operating Condition

The control effects of strategies are evaluated by the equalization time and energy consumption. The energy loss during the balancing process is the algebraic sum of the product of voltages and balancing currents. The calculation of energy loss can be expressed as:

$$loss = \sum_{t=T_1}^{T_2} \sum_{i=1}^{6} I_i(t) U_i(t) \Delta t \tag{46}$$

where T_1 and T_2 are start and stop moment of the balancing process, $I_i(t)$ is balancing current, $U_i(t)$ is terminal voltage of *Cell i*, Δt is sampling time and equal to 1 s.

Before equalization experiment, the tested cells were charged to specific voltages by CC-CV method with a cut-off current of 0.01 A. The initial voltages and SoCs of cells are shown in Table 5. Figure 8 displays the experiment result of FDC. The SoC curve of Cell 6 indicates that Cell 6 is discharged to a lower SoC 0.4609 then charged to the terminal SoC 0.4704. The phenomenon of redundant repeated charging and discharging leads to unnecessary energy transfer and consequently results in higher energy loss. Besides, those cells, which were discharged then charged, tend to age faster, enhancing the discrepancy of the battery string. A similar but weakened phenomenon can be observed in experiment result of VDC strategy, as shown in Figure 9. Compared with FDC, VDC can reduce energy loss while increasing the balancing time. Figure 10 shows the equalization process controlled by GPC. The discharging depth of Cell 6 is lessened, and SoC curves are smoother than FDC. Therefore, compared with FDC, GPC demonstrates improved performance. Figure 11 shows the experiment result of the VSSGPC. The phenomenon of unnecessarily repeated charging and discharging vanished, and much smoother SoC curves are obtained, leading to palliation of aging. The balancing currents are shown in Figure 12. Duty Cycles of control signals are shown in Figure 13.

Table 5. Initialization of tested cells.

Cell Number	1	2	3	4	5	6
Initial Voltage	3.7679 V	3.6204 V	3.6407 V	3.7300 V	3.8514 V	3.6915 V
Initial SoC	0.6000	0.4000	0.4260	0.5550	0.7000	0.5000

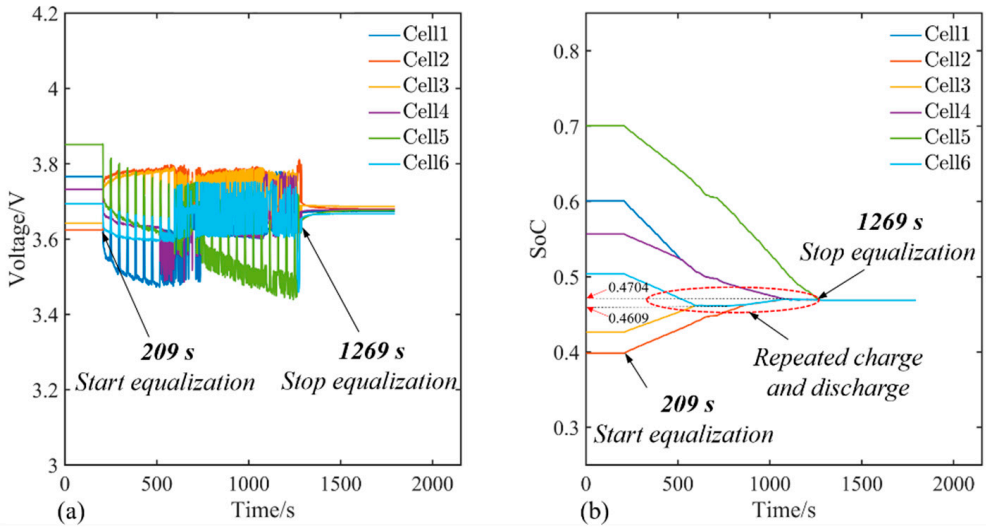

Figure 8. Equalization experiment based on FDC: (**a**) Voltage; (**b**) SoC.

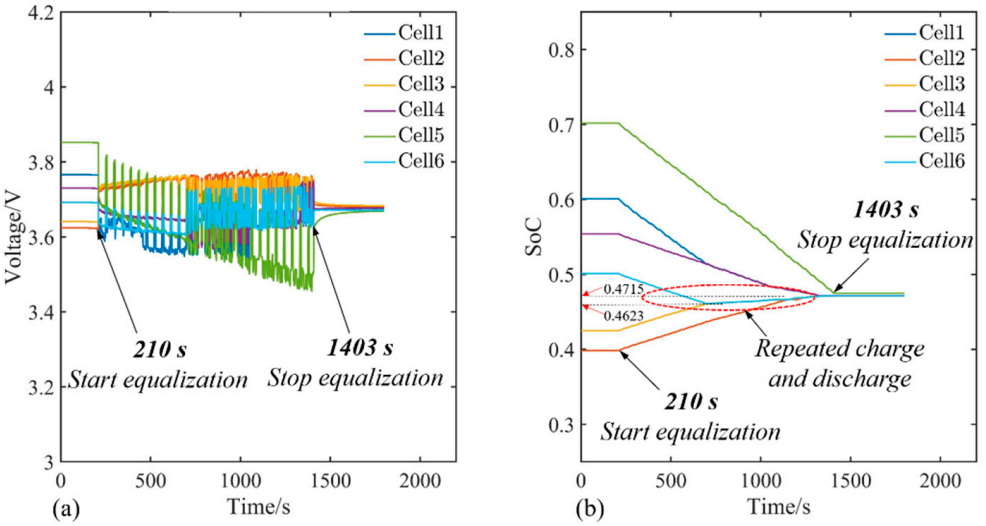

Figure 9. Equalization experiment based on VDC: (**a**) Voltage; (**b**) SoC.

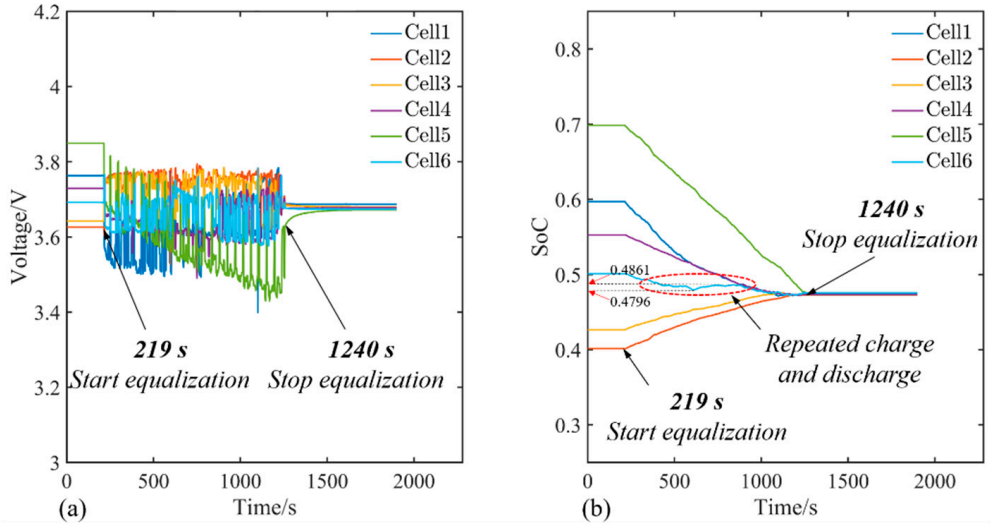

Figure 10. Equalization experiment based on GPC: (**a**) Voltage; (**b**) SoC.

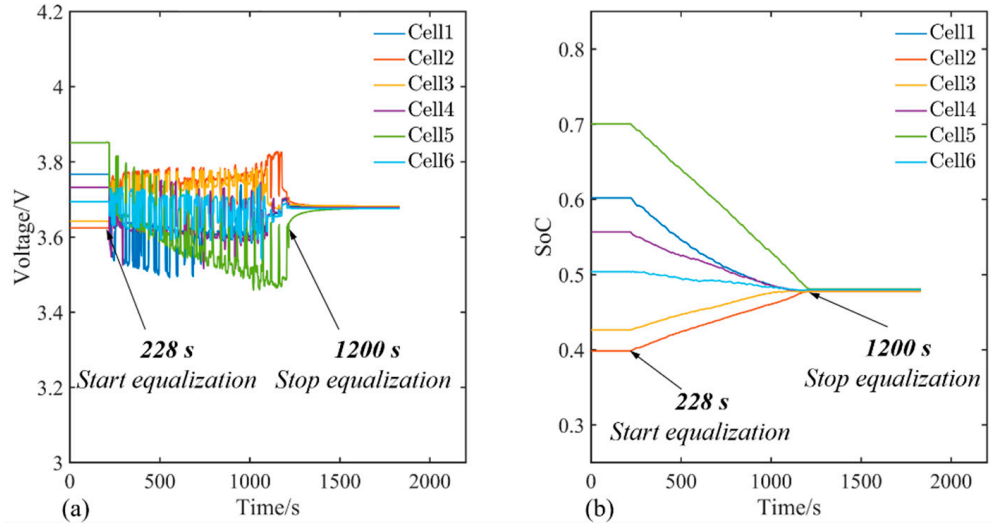

Figure 11. Equalization experiment based on VSSGPC: (**a**) Voltage; (**b**) SoC.

The experiment results are further evaluated in the aspect of equalization time, energy consumption and terminal average SoCs, which are summarized in Table 6. Compared with FDC, VDC reduces energy loss by 6.5% and yet increases equalization time by 12.5%. Therefore, VDC can reduce energy consumption at the cost of equalization time. In contrast with FDC, GPC shortens the equalization time by 3.7% and reduces the energy loss by 11.5%. Compared with FDC, VSSGPC shortens the equalization time by 8.3% and reduces energy loss by 16.5%. Hence, GPC improves the equalization procedure markedly, and VSSGPC further enhances the performance of equalizer.

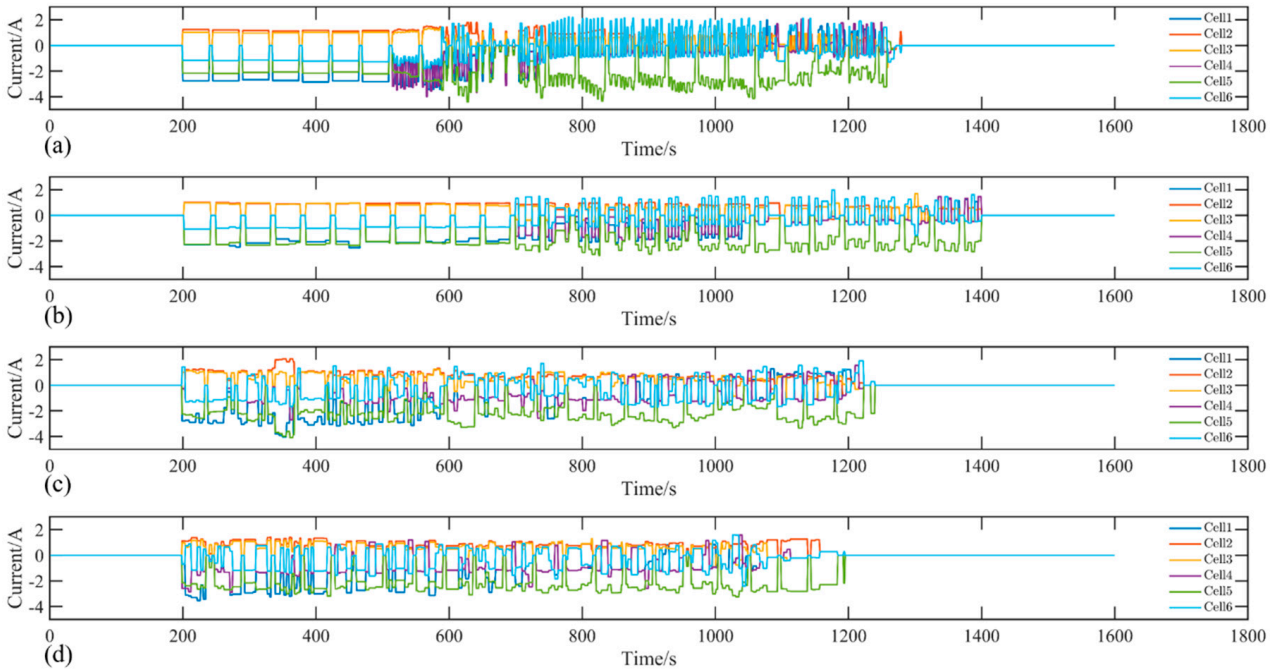

Figure 12. Balancing current: (**a**) FDC; (**b**) VDC; (**c**) GPC. (**d**) VSSGPC.

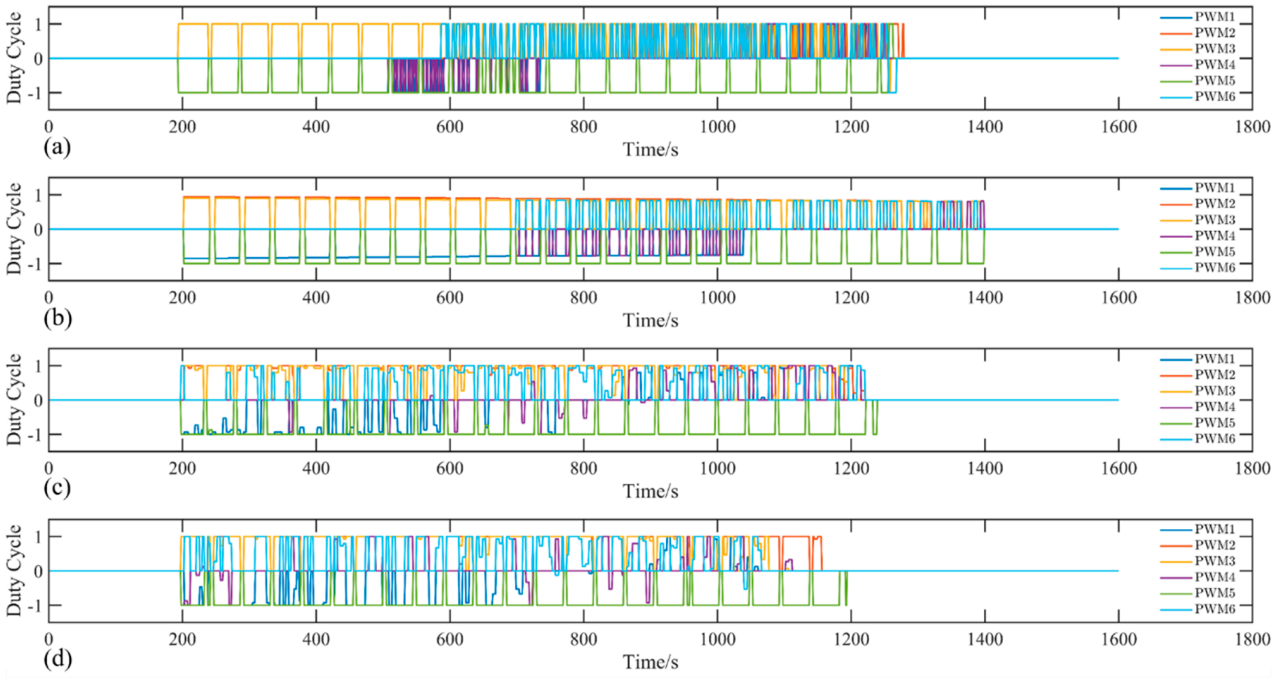

Figure 13. Duty Cycle of control signals: (**a**) FDC; (**b**) VDC; (**c**) GPC; (**d**) VSSGPC.

Table 6. Equalization experiment result.

Control Strategy.	FDC	VDC	GPC	VSSGPC
Equalization time (Comparison)	1060 s \	1193 (+12.5%)	1021 s (−3.7%)	972 s (−8.3%)
Terminal Average SoC	0.4686	0.4721	0.4740	0.4791
Energy Consumption (Comparison)	3.6115 W·h \	3.3807 W·h (−6.5%)	3.1944 W·h (−11.5%)	3.0154 W·h (−16.5%)

5.3. Charging and Discharging Operating Conditions

In order to demonstrate the adaptability of BFTE and VSSGPC strategy, equalization experiment based on VSSGPC is carried out in CC-CV and EUDC condition, respectively. As shown in Figure 14, VSSGPC strategy is applied in CC-CV charging condition. The initial SoCs are set to [0.35, 0.17, 0.20, 0.30, 0.45, 0.25] and the charging cut-off SoC is 0.90. Compared with CC-CV charging condition without equalization, the available capacity of the battery string is promoted from 7.755 A·h to 12.375 A·h. Figure 15 shows the result of equalization experiment based on VSSGPC in EUDC condition. The initial SoCs are set to [0.85, 0.65, 0.69, 0.80, 0.95, 0.75] and the discharging cut-off SoC is 0.15. Compared with EUDC discharging condition without equalization, the discharged capacity is promoted from 8.25 to 9.53 A·h. Since the equalizer and VSSGPC strategy are capable of operating in multiple operating conditions, their broad applicability is demonstrated. Table 7 summarizes the comparison of experiment results in charging and discharging conditions.

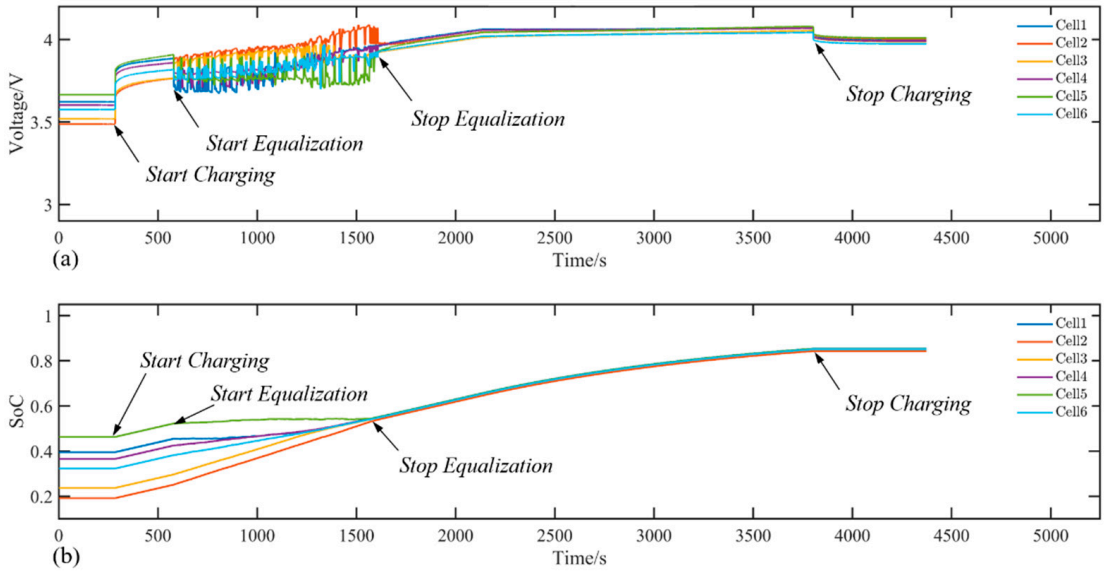

Figure 14. Equalization experiment based on VSSGPC strategy in CC-CV operating condition: (**a**) Voltage; (**b**) SoC.

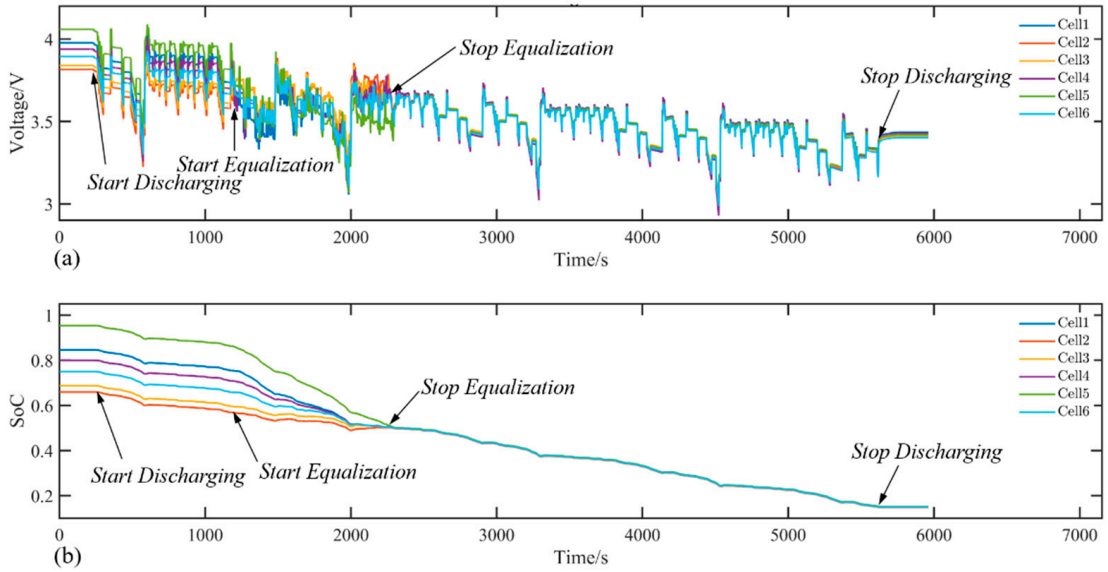

Figure 15. Equalization experiment based on VSSGPC strategy in EUDC operating condition: (**a**) Voltage; (**b**) SoC.

Table 7. Comparison of charging and discharging operating condition.

Conditions	Parameters	Without Equalization	With Equalization
CC-CV	Available SoC	0.47	0.75
	Available capacity (Comparison)	7.76 A·h \	12.38 A·h (+59.5%)
EUDC	Discharged SoC	0.50	\
	Discharged capacity (Comparison)	8.25 A·h \	9.53 A·h (+15.5%)

5.4. Discussion

5.4.1. The Advantage of BFTE

The experiment results indicate that BFTE is competent for string equalization. The advantages of BFTE are summarized as follows:

1. The electric isolation between cells, which is guaranteed by transformers, improves the security of the equalizer.
2. If glitches occur in one separate sub-module, the rest part of the equalizer can function as usual by reason of the modular design of the equalizer, which ensures the sub-modules independent from each other.
3. The bidirectionality of energy flow ensured by the BFTE realizes the flexible energy transition between cells and string, making it available for complex battery balancing requirements.

Benefit from the modular design of equalizer and independence of controlling PWM channels, multiple cells can be balanced synchronously, which enhances balancing efficiency dramatically. The experiment result indicates that BFTE is competent for static, charging and discharging conditions, which demonstrates its competency in various operating conditions.

5.4.2. The Superiority of VSSGPC

The rationality of the proposed VSSGPC strategy is analyzed theoretically on the basis of experiment results. A good equalization strategy should have the advantages of short balancing time and low equalization loss. The superiority is demonstrated by comparing with FDC and VDC methods mentioned in Section 1.

FDC employs stationary duty cycles thereby lacking the ability to regulate the balancing currents. Those cells whose SoCs are higher or lower than the average value are discharged or charged at the maximum equalization current, respectively. Consequently, the cells are repeatedly charged and discharge during the entire equalization process. FDC emerges the highest energy loss and life reduction.

VDC adopts changeable duty cycles and accordingly is capable of regulating the balancing current. Compared with FDC, the applied duty cycles of VDC are proportional to SoC deviations from the average value, rather than set to the maximum. Consequently, the characteristic of proportional duty cycles can lessen energy loss but VDC inevitably increases the equalization time due to the non-maximum duty cycle.

The major setbacks of FDC and VDC can be summarized by focusing on two aspects. Firstly, FDC and VDC only consider the terminal control target but ignore the processual control target. Secondly, the FDC and VDC are model-free methods and thus take no notice of the system characteristics, such as coupling and time-varying. As a consequence, the control effect is unsatisfactory.

GPC can address these drawbacks and are competent for equalization control due to the following three aspects.

1. Benefit from the feature of adaptive control, GPC is applicable for the parameter-under-determined or time-varying system. The model parameters can be initialized or adjusted before or during the control process. The characteristics of the system can be reflected in the identified model.
2. GPC is characterized by multi-step prediction. The embedded cost function concerning the predicted outputs reflects the processual control target. GPC considers both terminal control target and processual control target and thus demonstrates superior control effects.
3. GPC has the feature of rolling-optimization. The optimum control law in the present is calculated based on predicted outputs. As time moving forward, the global control process is optimized.

Benefit from the three advantages, GPC demonstrates a lower energy loss and faster equalization speed compared with FDC and VDC. However, a lighten phenomenon of unnecessarily repeated charge and discharge still can be observed due to the limited horizons and non-global optimization.

VSSGPC retains the advantages and competency of GPC. Furthermore, by introducing the Step Size Factor, the control and output horizons are enlarged, which enables global optimization of equalization process. Accordingly, VSSGPC eliminates the phenomenon of unnecessary repeated charge and discharge and thus demonstrates the lowest energy loss and shortest equalization time. Therefore, VSSGPC illustrates the best control effect and should be employed for the equalization process.

5.4.3. Implementation Cost

The implementation cost of BFTE is analyzed and compared with the switch shunting resistor equalizer, which is the most commonly and vastly used equalization method in EVs. Control chips, transformers, MOSFETs, diodes and resistors are the essential materials for practical application of BFTE. However, the major materials employed in switch shunting resistor equalizer only consists of MOSFETs and resistors. The implementation cost of the verification experiment in this study is discussed first. As shown in Table 8, for string of 6 cells, the total cost of BFTE is USD 61.7 while the total cost of switch shunting resistor equalizer is USD 7.2. However, battery packs consist of over 60 cells in a realistic set up. Under this circumstance, the materials cost of BFTE is as high as USD 617 while the cost of switch shunting resistor equalizer is USD 72. Therefore, the high cost is an obstacle to the practical application of BFTE.

Table 8. Implementation cost of BFTE and switch shunting resistor equalizer.

Methods	Materials	Part Type	Number [1]	Unit Price [2]/USD	Total Price/USD
BFTE	Control Chip	LTC3300-1	1	9.5	9.5
	Transformer	WURTH-750312504	6	4.9	29.4
	MOSFET	SiR882DP	6	1.9	11.4
		SiS892DN	6	1.1	6.6
	Diode	DFLS260	6	0.3	1.8
		DFLS1100	6	0.3	1.8
	Resistor	1206/0.008R	12	0.1	1.2
		Total for string of 6 cells			61.7
		Total for pack of 60 cells (Realistic set up)			617
Switch shunting resistor equalizer [7]	MOSFET	SiS892DN	6	1.1	6.6
	Resistor	1206/33R	6	0.1	0.6
		Total for string of 6 cells			7.2
		Total for pack of 60 cells (Realistic set up)			72

[1] Number is the component amount of BFTE for string of 6 cells. [2] Unit Price is collected from MOUSER ELECTRONICS.

6. Conclusions

This paper proposes an active equalization method based on bidirectional flyback transformer equalizer (BFTE) and variable step size generalized predictive control (VSSGPC) for series-connected batteries. The main conclusion remarks can be made below:

1. BFTE is designed and analyzed to achieve cells' consistency. The analysis indicates that BFTE is implementable and can be controlled by PWMs. BFTE has a high level of performance and is preferable due to its reliability, design flexibility, energy transfer bidirectionality, and high equalization speed.
2. GPC is derived and applied in BFTE. Compared with FDC and VDC, GPC can reduce energy consumption and shorten equalization time substantially due to its characteristics of adaptive control, multi-step prediction and rolling optimization.
3. VSSGPC is further improved on GPC. By introducing the Step Size Factor in GPC, the control and output horizons are expanded. VSSGPC strategy overcomes the local limitation of GPC and consequently emerges the lowest energy lost and the shortest equalization time.
4. The effectiveness of BFTE and VSSGPC is validated in CC-CV and EUDC conditions. Compared with no equalization, BFTE and VSSGPC strategy can enhance the available capacity in CC-CV condition and discharged capacity in EUDC condition, which demonstrates the competency in various operating conditions.

In conclusion, because of the high performance and the adaptability in multi-working conditions, the equalization method based on BFTE and VSSGPC provides a preferable alternative of active equalization application for the scientific community and should be employed in EVs to save energy. However, the proposed method does not consider the high implementation cost of BFTE and lacks verification in the large-scale battery pack. In the future, the cost will be considered and minimized to facilitate practical implementation. Then, the experimental verification of the proposed method will be conducted in the large-scale battery packs. Finally, the proposed method will be implemented in EVs.

Author Contributions: Conceptualization, J.C. and B.X.; software, J.C.; data curation, J.Z., J.C; writing—original draft preparation, J.C.; writing—review and editing, B.X.; visualization, J.Z.; funding acquisition, B.X. All authors have read and agreed to the published version of the manuscript.

Funding: This research was funded by the Shenzhen Economic, Trade, and Information Commission of Shenzhen Municipality Strategic Emerging Industries and Future Industrial Development "Innovation Chain + Industrial Chain" Project (2017) and the National Natural Science Foundation of China (Grant No. 51877120).

Institutional Review Board Statement: Not applicable.

Informed Consent Statement: Not applicable.

Data Availability Statement: Data is contained within the article.

Conflicts of Interest: The authors declare no conflict of interest.

References

1. Wachtmeister, M. Overview and Analysis of Environmental and Climate Policies in China's Automotive Sector. *J. Environ. Dev.* **2013**, *22*, 284–312. [CrossRef]
2. Du, J.Y.; Ouyang, M.G.; Chen, J.F. Prospects for Chinese electric vehicle technologies in 2016–2020: Ambition and rationality. *Energy* **2017**, *120*, 584–596. [CrossRef]
3. Scrosati, B.; Garche, J. Lithium batteries: Status, prospects and future. *J. Power Sources* **2010**, *195*, 2419–2430. [CrossRef]
4. Lu, L.G.; Han, X.B.; Li, J.Q.; Hua, J.F.; Ouyang, M.G. A review on the key issues for lithium-ion battery management in electric vehicles. *J. Power Sources* **2013**, *226*, 272–288. [CrossRef]
5. Uno, M.; Yashiro, K.; Hasegawa, K. Modularized Equalization Architecture with Voltage Multiplier-Based Cell Equalizer and Switchless Switched Capacitor Converter-Based Module Equalizer for Series-Connected Electric Double-Layer Capacitors. *IEEE Trans. Power Electron.* **2019**, *34*, 6356–6368. [CrossRef]
6. Chen, H.; Zhang, L.; Han, Y. System-theoretic analysis of a class of battery equalization systems: Mathematical modeling and performance evaluation. *IEEE Trans. Veh. Technol.* **2014**, *64*, 1445–1457. [CrossRef]
7. Hoque, M.M.; Hannan, M.A.; Mohamed, A.; Ayob, A. Battery charge equalization controller in electric vehicle applications: A review. *Renew. Sustain. Energy Rev.* **2017**, *75*, 1363–1385. [CrossRef]
8. Kutkut, N.H.; Divan, D.M. Dynamic equalization techniques for series battery stacks. In Proceedings of the Intelec'96-International Telecommunications Energy Conference, Adelaide, Australia, 23–25 May 1995; pp. 514–521.
9. Isaacson, M.; Hollandsworth, R.; Giampaoli, P.; Linkowsky, F.; Salim, A.; Teofilo, V. Advanced lithium ion battery charger. In Proceedings of the Fifteenth Annual Battery Conference on Applications and Advances (Cat. No. 00TH8490), Long Beach, CA, USA, 11–14 January 2000; pp. 193–198.
10. Pascual, C.; Krein, P.T. Switched capacitor system for automatic series battery equalization. In Proceedings of the APEC 97-Applied Power Electronics Conference, Atlanta, GA, USA, 27–27 February 1997; pp. 848–854.
11. Cao, J.; Schofield, N.; Emadi, A. Battery balancing methods: A comprehensive review. In Proceedings of the 2008 IEEE Vehicle Power and Propulsion Conference, Harbin, China, 3–5 September 2008; pp. 1–6.
12. Wang, X.L.; Cheng, K.W.E.; Fong, Y.C. Zero Current Switching Switched-Capacitors Balancing Circuit for Energy Storage Cell Equalization and Its Associated Hybrid Circuit with Classical Buck-Boost. *Energies* **2019**, *12*, 2726. [CrossRef]
13. Mohamed, D.; Noshin, O.; Peter, V.; Joeri, V. A review of passive and active battery balancing based on Matlab/Simulink. *Int. Rev. Electr. Eng.* **2011**, *6*, 2974–2989.
14. Daowd, M.; Omar, N.; Van Den Bossche, P.; Van Mierlo, J. Passive and active battery balancing comparison based on MATLAB simulation. In Proceedings of the 2011 IEEE Vehicle Power and Propulsion Conference, Chicago, IL, USA, 6–9 September 2011; pp. 1–7.
15. Baughman, A.C.; Ferdowsi, M. Double-tiered switched-capacitor battery charge equalization technique. *IEEE Trans. Ind. Electron.* **2008**, *55*, 2277–2285. [CrossRef]
16. Baughman, A.; Ferdowsi, M. Double-tiered capacitive shuttling method for balancing series-connected batteries. In Proceedings of the 2005 IEEE Vehicle Power and Propulsion Conference, Chicaco, IL, USA, 7–9 September 2005; pp. 109–113.
17. Park, S.-H.; Kim, T.-S.; Park, J.-S.; Moon, G.-W.; Yoon, M.-J. A new battery equalizer based on buck-boost topology. In Proceedings of the 2007 7th Internatonal Conference on Power Electronics, Daegu, Korea, 22–26 October 2007; pp. 962–965.
18. Phung, T.H.; Crebier, J.-C.; Chureau, A.; Collet, A.; Nguyen, V. Optimized structure for next-to-next balancing of series-connected lithium-ion cells. In Proceedings of the 2011 Twenty-Sixth Annual IEEE Applied Power Electronics Conference and Exposition (APEC), Fort Worth, TX, USA, 6–11 March 2011; pp. 1374–1381.
19. Cadar, D.V.; Petreus, D.M.; Patarau, T.M. An Energy Converter Method for Battery Cell Balancing. In Proceedings of the 2010 33rd International Spring Seminar on Electronics Technology (ISSE 2010), Warsaw, Poland, 12–16 May 2010; pp. 290–293. [CrossRef]
20. Shin, J.-W.; Seo, G.-S.; Chun, C.-Y.; Cho, B.-H. Selective flyback balancing circuit with improved balancing speed for series connected lithium-ion batteries. In Proceedings of the 2010 International Power Electronics Conference-ECCE ASIA, Sapporo, Japan, 21–24 June 2010; pp. 1180–1184.
21. Park, H.S.; Kim, C.H.; Park, K.B.; Moon, G.W.; Lee, J.H. Design of a Charge Equalizer Based on Battery Modularization. *IEEE Trans. Veh. Technol.* **2009**, *58*, 3216–3223. [CrossRef]
22. Song, S.X.; Xiao, F.; Peng, S.L.; Song, C.X.; Shao, Y.L. A High-Efficiency Bidirectional Active Balance for Electric Vehicle Battery Packs Based on Model Predictive Control. *Energies* **2018**, *11*, 3220. [CrossRef]
23. Shi, F.D.; Song, D.W. A Novel High-Efficiency Double-Input Bidirectional DC/DC Converter for Battery Cell-Voltage Equalizer with Flyback Transformer. *Electronics* **2019**, *8*, 1426. [CrossRef]
24. Hasan, R.; Mekhilef, S.; Seyedmahmoudian, M.; Horan, B. Grid-connected isolated PV microinverters: A review. *Renew. Sustain. Energy Rev.* **2017**, *67*, 1065–1080. [CrossRef]

25. Gopi, R.R.; Sreejith, S. Converter topologies in photovoltaic applications—A review. *Renew. Sustain. Energy Rev.* **2018**, *94*, 1–14. [CrossRef]
26. Bizhong, X.; Jie, Z.; Yadi, Y.; Huawen, W.; Wei, W.; Yongzhi, L. A Novel Battery Equalization Method Base on Fuzzy Logic Control Considering Thermal Effect. *IOP Conf. Ser. Earth Environ. Sci.* **2019**, *300*. [CrossRef]
27. Lim, C.-S.; Lee, K.-J.; Ku, N.-J.; Hyun, D.-S.; Kim, R.-Y. A modularized equalization method based on magnetizing energy for a series-connected lithium-ion battery string. *IEEE Trans. Power Electron.* **2013**, *29*, 1791–1799. [CrossRef]
28. Liu, X.; Sun, Y.; He, Y.; Zheng, X.; Zeng, G.; Zhang, J. Battery equalization by fly-back transformers with inductance, capacitance and diode absorbing circuits. *Energies* **2017**, *10*, 1482. [CrossRef]
29. Kim, M.Y.; Kim, J.H.; Moon, G.W. Center-Cell Concentration Structure of a Cell-to-Cell Balancing Circuit With a Reduced Number of Switches. *IEEE Trans. Power Electron.* **2014**, *29*, 5285–5297. [CrossRef]
30. Hua, C.C.; Fang, Y.H. A Charge Equalizer with a Combination of APWM and PFM Control Based on a Modified Half-Bridge Converter. *IEEE Trans. Power Electron.* **2016**, *31*, 2970–2979. [CrossRef]
31. Wang, S.C.; Liu, C.Y.; Liu, Y.H. A Fast Equalizer with Adaptive Balancing Current Control. *Energies* **2018**, *11*, 1052. [CrossRef]
32. Yan, J.; Cheng, Z.; Xu, G.; Qian, H.; Xu, Y. Fuzzy control for battery equalization based on state of charge. In Proceedings of the 2010 IEEE 72nd Vehicular Technology Conference-Fall, Ottawa, ON, Canada, 6–9 September 2010; pp. 1–7.
33. Zheng, L.; Zhu, J.; Wang, G.; Lu, D.D.-C.; McLean, P.; He, T. Model predictive control based balancing strategy for series-connected lithium-ion battery packs. In Proceedings of the 2017 19th European conference on power electronics and applications (EPE'17 ECCE Europe), Warsaw, Poland, 11–14 September 2017; pp. 1–8.
34. Wang, J.Y.; Dai, S.L.; Chen, X.; Zhang, X.; Shan, Z.F. Bidirectional Multi-Input and Multi-Output Energy Equalization Circuit for the Li-Ion Battery String Based on the Game Theory. *Complexity* **2019**. [CrossRef]
35. Tavakoli, A.; Khajehoddin, S.A.; Salmon, J. Control and Analysis of a Modular Bridge for Battery Cell Voltage Balancing. *IEEE Trans. Power Electron.* **2018**, *33*, 9722–9733. [CrossRef]
36. Wu, X.G.; Cui, Z.H.; Li, X.F.; Du, J.Y.; Liu, Y. Control Strategy for Active Hierarchical Equalization Circuits of Series Battery Packs. *Energies* **2019**, *12*, 2071. [CrossRef]
37. Wang, Y.; Zhang, C.; Chen, Z.; Xie, J.; Zhang, X. A novel active equalization method for lithium-ion batteries in electric vehicles. *Appl. Energy* **2015**, *145*, 36–42. [CrossRef]
38. Zheng, Y.; Ouyang, M.; Lu, L.; Li, J.; Han, X.; Xu, L. On-line equalization for lithium-ion battery packs based on charging cell voltages: Part 1. Equalization based on remaining charging capacity estimation. *J. Power Sources* **2014**, *247*, 676–686. [CrossRef]
39. Ma, Y.; Duan, P.; Sun, Y.S.; Chen, H. Equalization of Lithium-Ion Battery Pack Based on Fuzzy Logic Control in Electric Vehicle. *IEEE Trans. Ind. Electron.* **2018**, *65*, 6762–6771. [CrossRef]
40. Lin, C.; Mu, H.; Zhao, L.; Cao, W.K. A New Data-Stream-Mining-Based Battery Equalization Method. *Energies* **2015**, *8*, 6543–6565. [CrossRef]
41. Wang, R.; Lukic, S.M. Review of driving conditions prediction and driving style recognition based control algorithms for hybrid electric vehicles. In Proceedings of the 2011 IEEE Vehicle Power and Propulsion Conference, Chicago, IL, USA, 6–9 September 2011; pp. 1–7.
42. Hussein, A.A.-H.; Batarseh, I. A review of charging algorithms for nickel and lithium battery chargers. *IEEE Trans. Veh. Technol.* **2011**, *60*, 830–838. [CrossRef]
43. Arora, S.; Shen, W.; Kapoor, A. Review of mechanical design and strategic placement technique of a robust battery pack for electric vehicles. *Renew. Sustain. Energy Rev.* **2016**, *60*, 1319–1331. [CrossRef]
44. Clarke, D.W.; Mohtadi, C.; Tuffs, P. Generalized predictive control—Part I. The basic algorithm. *Automatica* **1987**, *23*, 137–148. [CrossRef]